Am J Transl Res 2026;18(2):1414-1430
www.ajtr.org /ISSN:1943-8141/AJTR0169093

Original Article

M2 macrophage-secreted exosomal miR-216a regulates microglial polarization by targeting the HMGB1/TLR4/NF-κB pathway to alleviate bone cancer pain

Shilin Cao[1*], Haihe Yang[2*], Peiyao Li[1], Xiangming Li[1], Simin Shen[1], Qianye Li[1], Zhangxiang Huang[1]

[1]*Department of Pain, First Affiliated Hospital of Kunming Medical University, Kunming 650000, Yunnan, China;* [2]*Department of Pain Treatment, Lincang People's Hospital, Lincang 677000, Yunnan, China.* [*]*Equal contributors.*

Received September 30, 2025; Accepted December 11, 2025; Epub February 15, 2026; Published February 28, 2026

Abstract: Objective: M2 macrophage-derived exosomes (M2-exos) hold promise for patients with bone cancer pain (BCP). This study aimed to investigate the therapeutic effect and related mechanisms of M2-exos in both in vitro and in vivo models of BCP. Method: RAW 264.7 macrophages were treated with IL-4 to generate M2-polarized macrophages. M2-exos were characterized by transmission electron microscope and Western blotting. A mouse model of BCP was established, and BV2 microglia were activated by lipopolysaccharide stimulation. The effects of M2-exos were evaluated in vitro by coculture with reactive BV2 microglia and in vivo by microinjection into the rostral ventromedial medulla (RVM) of BCP mice. CCK-8 assays, ELISAs, flow cytometry and immunofluorescence were used to determine the effects of M2-exos on microglial activation. The therapeutic effects of M2-exos were evaluated via pain behavior experiments. Bioinformatic analysis and rescue experiments were performed to investigate the mechanisms through which M2-exos affect the progression of BCP. Results: In vitro, M2-exos administration repolarized microglial toward the anti-inflammatory M2 phenotype in coculture systems. In vivo analysis indicated that microinjection of M2-exos into the RVM region improved neuroinflammation. Notably, miR-216a expression was significantly increased in M2-exos and could be delivered into BV2 microglia. Blockade of miR-216a abolished the therapeutic effects of M2-exos in vitro and in vivo. Mechanistically, miR-216a negatively regulates high mobility group Box 1 protein (HMGB1) expression, further inhibiting Toll-like receptor 4 (TLR4)/NF-κB and inducing M2 microglial polarization, thereby delaying BCP progression. Conclusion: M2 macrophage-derived exosomal miR-216a could delay BCP progression by targeting HMGB1/TLR4/NF-κB-mediated microglial M2 polarization.

Keywords: Bone cancer pain (BCP), exosome, M2 macrophage, miR-216a, rostral ventromedial medulla (RVM)

Introduction

Bone cancer pain (BCP) is among the most prevalent forms of pain among cancer patients and is typically persistent, sudden, and spontaneous. BCP is a major contributor to patient suffering in advanced stages of cancer and significantly impairs the quality of life and self-efficacy of cancer survivors [1]. The etiology and pathophysiological mechanisms of BCP are highly complex and involve tumor-induced bone destruction, peripheral sensory system hyperalgesia, and central nervous system hyperalgesia [2-4]. However, the precise mechanisms underlying BCP remain incompletely understood. Current clinical interventions for BCP, including pharmacotherapy, radiotherapy, chemotherapy and nerve blocks, lack specificity and have not yielded satisfactory pain management outcomes [5-7]. Therefore, further investigations into the underlying mechanisms and the identification of novel therapeutic targets are essential for the development of effective BCP treatments.

The rostral ventromedial medulla (RVM) is a critical component of the brainstem's descending pain modulation system. It originates from the reticular formation and plays a central role in the initiation and maintenance of neuropathic pain. In BCP models, microglia in the RVM are markedly activated [8]. The inhibition of microglial activation in the RVM was shown to alleviate BCP progression [9]. As resident macrophages

within the central nervous system, microglia exhibit remarkable plasticity [10]. Upon exposure to various stimuli, microglia can polarize into two major phenotypes: proinflammatory (M1) and anti-inflammatory (M2) [11]. Proinflammatory cytokines secreted by M1-polarized microglia can activate neighboring neurons, contributing to central sensitization, whereas M2-polarized microglia secrete anti-inflammatory mediators that promote immune homeostasis and alleviate pain [12]. The polarization of microglia is closely associated with the progression of BCP and could be a new therapeutic target [13].

Exosomes are extracellular vesicles derived from the endocytic pathway with diameters ranging from 30 to 150 nm. Exosomes contain a variety of bioactive molecules, including small RNAs (miRNAs), mRNAs, and proteins, and their functional properties are determined by their cellular origin and molecular cargo [14, 15]. Exosomes are secreted by almost all cell types, including cancer cells, mesenchymal stem cells, neurons and macrophages [16-19]. In the extracellular environment, exosomes can interact with target cells through receptor-mediated adhesion, followed by internalization via endocytosis or direct membrane fusion, ultimately delivering their contents into recipient cells [20]. The favorable biological properties of exosomes include their low toxicity, low immunogenicity and high engineerability. Thus, exosome-based therapies have been intensively investigated. Numerous studies have demonstrated that exosomes hold promise as cell-free therapies for pain relief [21]. However, whether M2 macrophage-derived exosomes (M2-exos) delay BCP progression requires further investigation.

In this study, we aimed to determine the therapeutic effect of M2-exos on BCP and the related mechanism. M2-exos alleviated symptoms of BCP in mice in vivo and attenuated the LPS-induced activation of BV-2 cells in vitro. We also revealed that M2-exos could induce M2 microglial polarization via the secretion of miR-216a, thereby regulating the high mobility group Box 1 protein (HMGB1)/TLR4 (Toll-like receptor 4)/NF-κB pathway and ultimately alleviating the progression of BCP.

Materials and methods

Cell culture, treatment and transfection

RAW264.7 macrophages and BV2 cells were obtained from the Cell Bank of the Chinese Academy of Sciences (Shanghai, China). RAW-264.7 cells were cultured in high-glucose Dulbecco's modified Eagle's medium (DMEM; Thermo Fisher) supplemented with 10% fetal bovine serum (FBS; Gibco) and 100 U/ml penicillin and streptomycin. BV2 cells were cultured in DMEM supplemented with 10% FBS and 1% penicillin-streptomycin. The cells were incubated at 37°C with 5% CO_2.

RAW264.7 macrophages were polarized to the M2 phenotype by stimulation with interleukin 4 (IL-4, 20 ng/mL). Lipopolysaccharide (LPS; 100 ng/mL) was used to stimulate the BV2 cells.

The miR-216a inhibitor and NC inhibitor (10 nM; RiboBio) were transfected into M2 macrophages using Lipofectamine 3000 (Thermo Fisher) to downregulate the expression of miR-216a. At 48 h after transfection, the M2 macrophage supernatant was collected for exosome isolation.

Exosome extraction and identification

Exosomes were isolated from the collected M2 macrophage culture medium through ultracentrifugation. First, the culture medium was centrifuged at 4°C and 2000×g for 20 min, after which the supernatant was collected, and the pellet was discarded. The supernatant was subsequently subjected to centrifugation at 4°C and 10,000×g for 40 min, after which the supernatant was collected, and the resulting pellet was discarded. The supernatant was then filtered using a 0.22 μm filter, and the filtrate was ultracentrifuged at 4°C and 110,000×g for 70 min. The supernatant was discarded, and the pellet was retained. The pellet was resuspended in PBS, followed by ultracentrifugation at 4°C and 110,000×g for 70 min. After removal of the supernatant, the exosomal pellet was resuspended in an appropriate volume of PBS and stored at 4°C for subsequent experiments.

Exosomes were identified by detecting the expression of the marker proteins CD9, CD81,

CD63, TSG101 and Calnexin by Western blotting. The morphology of the exosomes was identified using a transmission electron microscope. Exosome samples were fixed with 2% (v/v) paraformaldehyde for 30 min and then dropped onto a carbon-coated copper grid. The samples were negatively stained twice with 1% (w/v) uranyl acetate before image acquisition.

Exosome uptake assay

Exosomes (50 μg/mL) were added to recipient BV2 cells. Exosomes were stained with PKH26 and added to the BV2 cell media. After 24 h, fluorescence was detected under a fluorescence microscope.

CCK-8 assay

Cell viability was evaluated using the CCK-8 assay according to the manufacturer's instructions. Exosome-treated BV2 cells were seeded into 96-well plates for 24 h, after which 10 μL of CCK8 reagent (Beyotime) was added to each well. After 4 h, the absorbance at 450 nm was measured using a microplate reader.

ELISA

The cell supernatants were collected and analyzed using an IL-6 and TNF-α kit (Beyotime) according to the manufacturer's instructions. The absorbance at 450 nm was measured using a microplate reader.

Western blotting

The concentrations of proteins extracted from exosomes, cells and tissues were measured with a BCA kit (Beyotime). A sample loading system containing 25 μg of protein was prepared, and the proteins were separated by SDS-PAGE and transferred to a polyvinylidene fluoride (PVDF) membrane. After blocking with 5% skim milk or 5% bovine serum albumin (BSA; Solarbio), the membrane was probed with the following primary antibodies: anti-CD63 (1:2000; Abcam), anti-CD9 (1:1000; Abcam), anti-81 (1:1000; Abcam), anti-TSG101 (1:1000; Abcam), anti-Calnexin (1:1000; Beyotime), anti-Iba-1 (1:1000; Abcam), anti-HMGB1 (1:2000; Abcam), anti-TLR4 (1:1000; Abcam), anti-p65 (1:1000; Abcam), anti-p-p65 (1:2000; Abcam), and anti-GAPDH (1:5000; Proteintech). After the primary antibodies were removed, the membranes were washed with TBST and incubated with HRP-conjugated secondary antibodies (anti-rabbit, 1:5000; anti-mouse, 1:4000; Proteintech). After incubation, the membranes were washed with TBST, and a chemiluminescence kit (Thermo Fisher) was used to visualize the immunoreactivity of the target proteins. Quantitative data were analyzed using ImageJ software (ImageJ).

qPCR

The expression of miR-216a, IL-6 and TNF-α was analyzed by qPCR. Total RNA was extracted from the RVM samples using TRIzol reagent (Invitrogen, USA) according to the manufacturer's instructions. Complementary DNA (cDNA) was synthesized from mRNA with a PrimeScript RT reagent kit (Takara). For miRNAs, reverse transcription was conducted using the miRNA First Strand cDNA Synthesis kit (Sangon). qPCR was performed using a SYBR Premix Ex Taq II Kit (Takara) following the manufacturer's recommended protocol. The transcript levels of mRNA and miRNA were normalized to those of GAPDH and U6, respectively. Relative RNA expression was determined using the standard $2^{-\Delta\Delta Ct}$ method. The following primers were used:

IL-10 F: 5'-CCAAGCCTTATCGGAAATGA-3', R: 5'-TTTTCACAGGGGAGAAATCG-3'; TNF-α F: 5'-CCACCACGCTCTTCTGTCTAC-3', R: 5'-AGGGTCTGGGCCATAGAACT-3'; GAPDH F: 5'TTCAACGGCACAGTCAAGG-3', R: 5'-CACCAGTGGATGCAGGGAT-3'; miR-216a; F: 5'-TGTCGCAAATCTCTGCAGG-3', R: 5'-CAGAGCAGGGTCCGAGGTA 3'; and U6 F: 5'-CTCGCTTCGGCAGCACA-3', R: 5'-ACGCTTCAC GAATTTGCGT-3'.

Flow cytometry

Flow cytometry was used to assess the expression of RAW 264.7 cell and BV2 cell surface markers. IL-4-stimulated RAW 264.7 macrophages were incubated with F4/80-PE (Thermo Fisher Scientific) and CD206-APC (BD Pharmingen) at 4°C in the dark for 30 min. LPS- and exosome-treated BV2 cells were incubated with a PE-conjugated anti-mouse CD206 antibody (BD Pharmingen) at 4°C in the dark for 30 min. A CytoFLEX flow cytometer was used for analysis.

Dual-luciferase reporter assay

Plasmid vectors containing the wild-type and mutant HMGB1 3' UTR with predicted miR-

216a binding sites were constructed. HEK-293 T cells were seeded into a 96-well plate and co-transfected with either the wild-type or mutant luciferase plasmids. After 48 h, the luciferase activity was assessed using a dual luciferase kit (Promega).

Animal experiments

Eight-week-old male C57BL/6 mice (20-25 g) were provided by Beijing Weitong Lihua Laboratory Animal Technology Co., Ltd. Mice were housed in a controlled environment with a room temperature of 22-26°C and humidity maintained at 70-80%. A 12-hour light/dark cycle was implemented, and the mice were allowed free access to food and water. The animal experiments conformed to the Guide for the Care and Use of Laboratory Animals. The Committee of Animal Care and Use of Kunming Medical University approved this study (Approval No. kmmu2021424). The procedures were conducted in accordance with the National Institutes of Health's Guide for the Care and Use of Laboratory Animals and the ARRIVE (Animal Research: Reporting In Vivo Experiments) guidelines.

To generate a BCP model, the mice were anesthetized via intraperitoneal injection of 50 mg/kg pentobarbital sodium. After routine disinfection and draping, the femoral plateau of the left knee joint was exposed using ophthalmic scissors. A small concave hole was created between the medial and lateral condyles using a fine needle, and the osteocortex was punctured with a dental drill.

In the sham group, 10 μL of heat-inactivated Lewis lung carcinoma (LLC) cells was injected into the left femoral cavity of each mouse. In the BCP group, 10 μL of Walker-256 breast cancer cells were injected into the left femoral cavity of each mouse. The injection site was sealed with bone wax. The wound was rinsed with normal saline, treated with penicillin powder, and then sutured.

To explore exosome function in vivo, exosomes (200 μg/mouse) were microinjected into the RVM as described in our previous study [8].

Mechanical pain test

The mice were placed in acrylic observation chambers with a wire mesh floor. Testing commenced after a 30-min acclimatization period. von Frey filaments were applied perpendicularly to the central region of the right hind paw for 6-8 sec. A positive response was defined as paw withdrawal or licking in response to the stimulus. Each filament was tested five times with an interval of at least 10 sec between trials. The minimum filament force required to elicit at least three positive responses was recorded as the paw withdrawal mechanical threshold (PWMT).

RVM sample collection

Immediately after the behavioral pain tests were completed, the mice were euthanized under chloral hydrate anesthesia. On an ice-cooled surface, the skin and fascia were incised, the neck muscles were dissected, and the skull was carefully opened using forceps. The brain and cerebellum were removed to expose the medulla oblongata, which was then sectioned at the upper and lower boundaries. The sampling area was defined as the area between the abducens nerve and the inferior cerebellar artery.

Immunofluorescence staining

For immunofluorescence staining, cells were fixed with 4% paraformaldehyde at 4°C for 30 min, permeabilized by incubation in 0.05% Triton X-100 solution and then blocked with 5% BSA. Cells were stained with anti-CD206 (Thermo Fisher), anti-Iba-1 (Thermo Fisher) and anti-F4/80 (Thermo Fisher) antibodies in the dark at room temperature for 30 min. The cells were then incubated with the appropriate secondary antibodies. The nuclei were stained with DAPI. Fluorescence images were then acquired under a fluorescence microscope.

For tissue immunofluorescence staining, the RVM sections were incubated in a blocking solution containing 10% BSA and 0.3% Triton X-100. The blocking solution was gently removed, and the sections were stained with anti-Iba1 (Thermo Fisher), anti-iNOS (Thermo Fisher), anti-206 (Thermo Fisher), anti-HMGB1 (Abcam), anti-TLR4 (Abcam) and anti-p65 (Abcam) antibodies. The corresponding fluorescent secondary antibodies were subsequently applied. Images of the RVM sections were captured using a confocal fluorescence microscope.

Statistical analysis

Statistical analysis was performed using GraphPad Prism 6.0. All the data are presented as the mean ± standard deviation (mean ± SD). Student's t test was used to assess the significance of the differences between the experimental and control groups. Statistical comparisons of more than two groups were carried out using one-way analysis of variance with the Bonferroni post hoc correction. A p value < 0.05 was considered to indicate statistical significance.

Results

Identification of M2 macrophages and M2-exos

RAW264.7 macrophages were polarized to the M2 phenotype by stimulation with IL-4. M2 macrophages were analyzed by light microscopy. M2-like macrophages were significantly enlarged and appeared mainly as round cells (**Figure 1A**) and subjected to flow cytometry (**Figure 1B**). Exosomes were isolated from M2 macrophages. The morphology and phenotypes of M2-exos were subsequently characterized. The results indicated that compared with M2 macrophages, M2-exos were enriched in TSG101, CD63, CD81 and CD9; in contrast, calnexin was barely detected (**Figure 1C**). The morphology of M2-exos was further analyzed by TEM (**Figure 1D**).

M2-exos attenuated LPS-induced inflammation in microglia and promoted M2 microglia polarization

We first investigated the effects of M2-exos on the viability, inflammatory cytokine release and M2 polarization of microglia. A neuroinflammation model was established using LPS-treated BV-2 cells in vitro, as confirmed by the increased expression of Iba-1 (**Figure 2A**). M2-exos were labeled with PKH67 dye and incubated with LPS-stimulated BV2 cells. As shown in **Figure 2B**, M2-exos were effectively internalized. Following LPS stimulation, BV2 cell viability was significantly reduced; however, treatment with M2-exos promoted the recovery of cell activity (**Figure 2C**). Moreover, LPS inhibited M2 macrophage polarization, whereas exosome administration induced M2 polarization (**Figure 2D** and **2E**). Furthermore, M2-exos suppressed the expression of proinflammatory cytokines (**Figure 2F** and **2G**).

M2-exos delayed BCP progression in mice

To evaluate the role of M2-exos in BCP, a mouse model of BCP was established by tumor cell injection (**Figure 3A**). Following successful model establishment, M2-exos were administered via intrathecal injection. As shown in **Figure 3B**, M2-exo treatment significantly alleviated pain symptoms in mice with BCP. The activation of microglia in the RVM was suppressed following M2-Exo treatment (**Figure 3C** and **3D**). A decrease in the expression of CD206, a marker of M2 macrophages, was observed (**Figure 3E**). In contrast, the M1 macrophage marker iNOS was upregulated in mice with BCP and suppressed upon M2-Exo administration (**Figure 3F**). Furthermore, M2-Exo treatment reduced the expression of proinflammatory cytokines (**Figure 3G** and **3H**).

M2-exos transport miR-216a into BV2 cells and promote M2 polarization

To elucidate the molecular mechanism by which M2-exos alleviate BCP progression, miRNA microarray and RNAlocate analyses were performed [22]. On the basis of previous findings, miR-216a was identified as a potential mediator of M2-exos-induced alleviation of BCP. qPCR demonstrated that the expression of miR-216a was significantly upregulated in M2-Exos (**Figure 4A**) and markedly increased in BV2 cells following M2-Exo treatment (**Figure 4B**). To validate the functional role of miR-216a in the inflammatory activity of microglia, we transfected miR-216a inhibitors into macrophages and subsequently collected their exosomes (**Figure 4C** and **4D**). However, inhibition of miR-216a failed to restore the viability of LPS-treated BV2 cells (**Figure 4E**). The results revealed that miR-216a knockdown suppressed M2 macrophage polarization (**Figure 4F** and **4G**) and increased the expression of inflammatory factors (**Figure 4H** and **4I**).

Exosomal miR-216a inhibited pain hypersensitivity and M2 polarization in mice with BCP

To confirm the role of exosomal miR-216a in BCP mice, we first analyzed the expression of miR-216a in the RVM of sham mice, BCP mice and M2-exo-treated BCP mice. The level of miR-

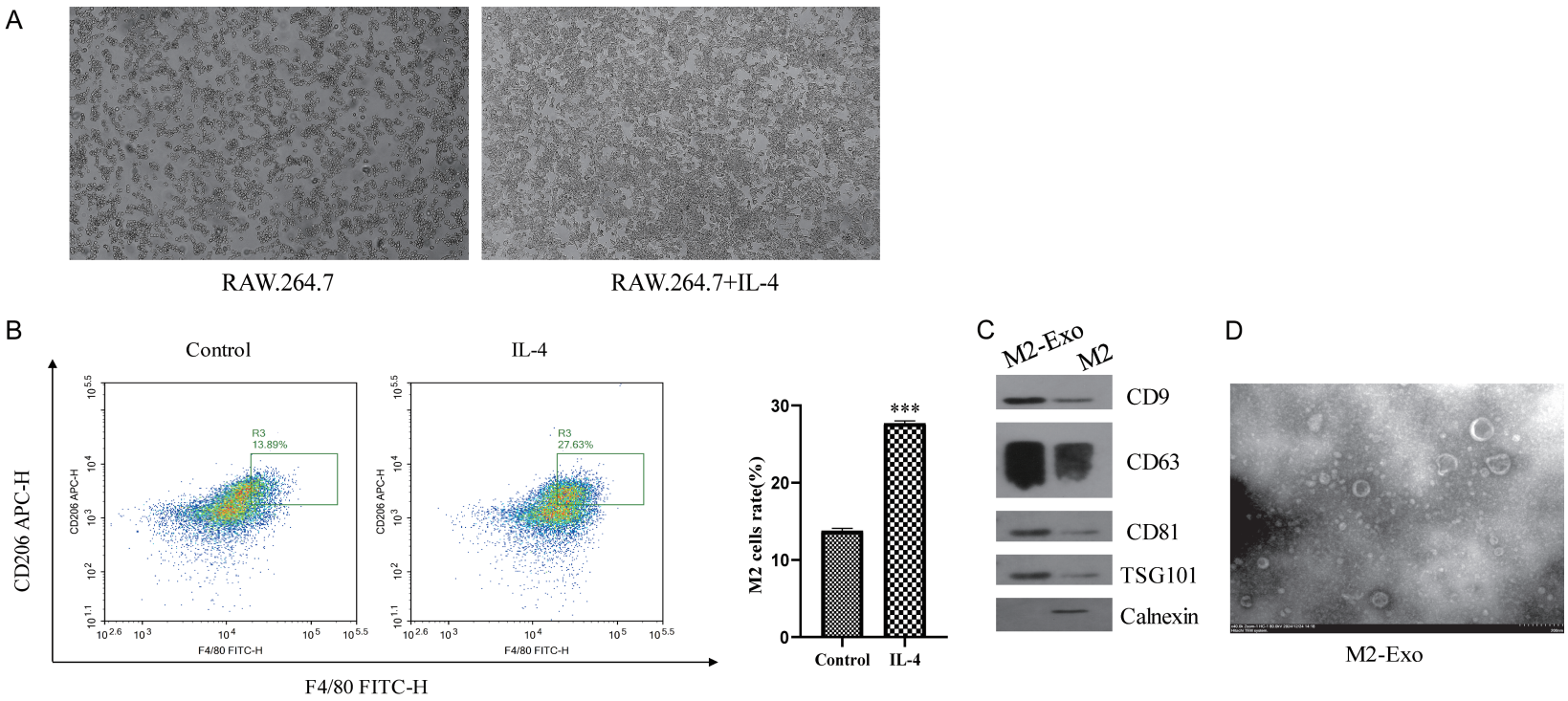

Figure 1. Identification of M2 macrophages and M2-exos. A. Cellular morphology analyzed by light microscopy. B. Expression and quantitative analysis of CD206 markers in IL-4-stimulated RAW264.7 cells assessed by flow cytometry. C. Western blot analysis of the expression of the exosomal markers CD9, CD63, CD81 and TSG101 in M2-exos. D. TEM analysis of M2-exos. Scale bars: 200 nm. ***P < 0.001.

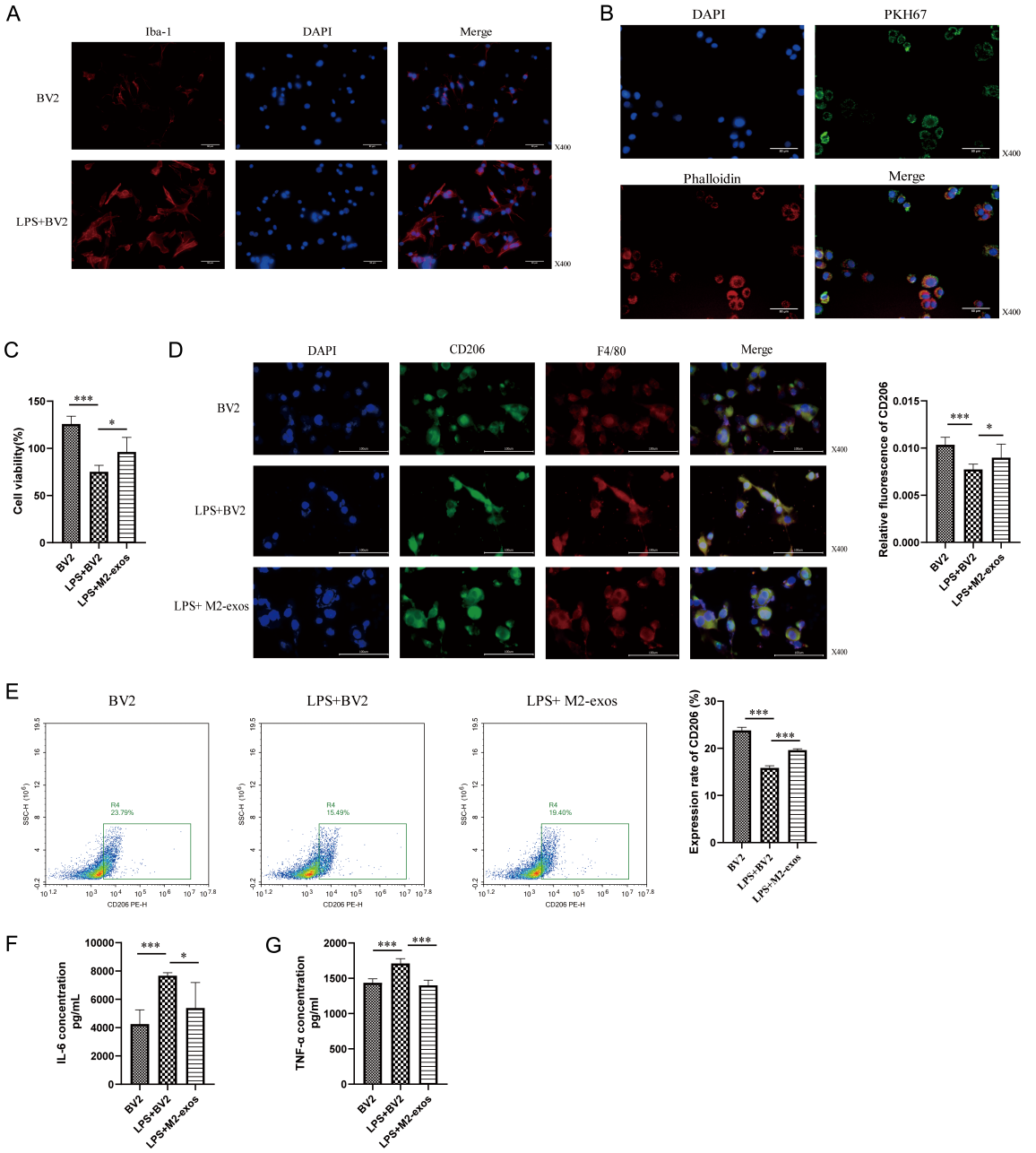

Figure 2. M2-exos attenuated LPS-induced inflammation in microglia and promoted M2 microglial polarization. A. The expression of Iba-1 in LPS-induced BV2 microglia detected by immunofluorescence, scale bars: 50 μm. B. PKH67-labeled M2-exos were taken up by BV2 cells, scale bars: 50 μm. C. The viability of LPS-induced BV2 microglia detected by a CCK-8 assay. D. Immunofluorescence staining of CD206 in BV2 cells, scale bars: 100 μm. E. The percentage of M2 macrophages was assessed by flow cytometry. F. The concentration of IL-6 released by BV2 cells was detected by ELISA. G. The concentration of TNF-α released by BV2 cells was detected by ELISA. The data are presented as the mean ± SD; $^{*}P < 0.05$, $^{***}P < 0.001$; n = 3.

216a in mice with BCP was reduced, while M2-exos treatment upregulated its expression (**Figure 5A**). Subsequently, BCP mice were treated with miR-216a-deficient M2-exos (**Figure 5B**). As shown in **Figure 5C**, the PWMT in mice decreased following miR-216a inhibition. Moreover, miR-216a knockdown failed to suppress microglial activation (**Figure 5D**) or promote M2 macrophage polarization (**Figure 5E**). Notably, the secretion of inflammatory cyto-

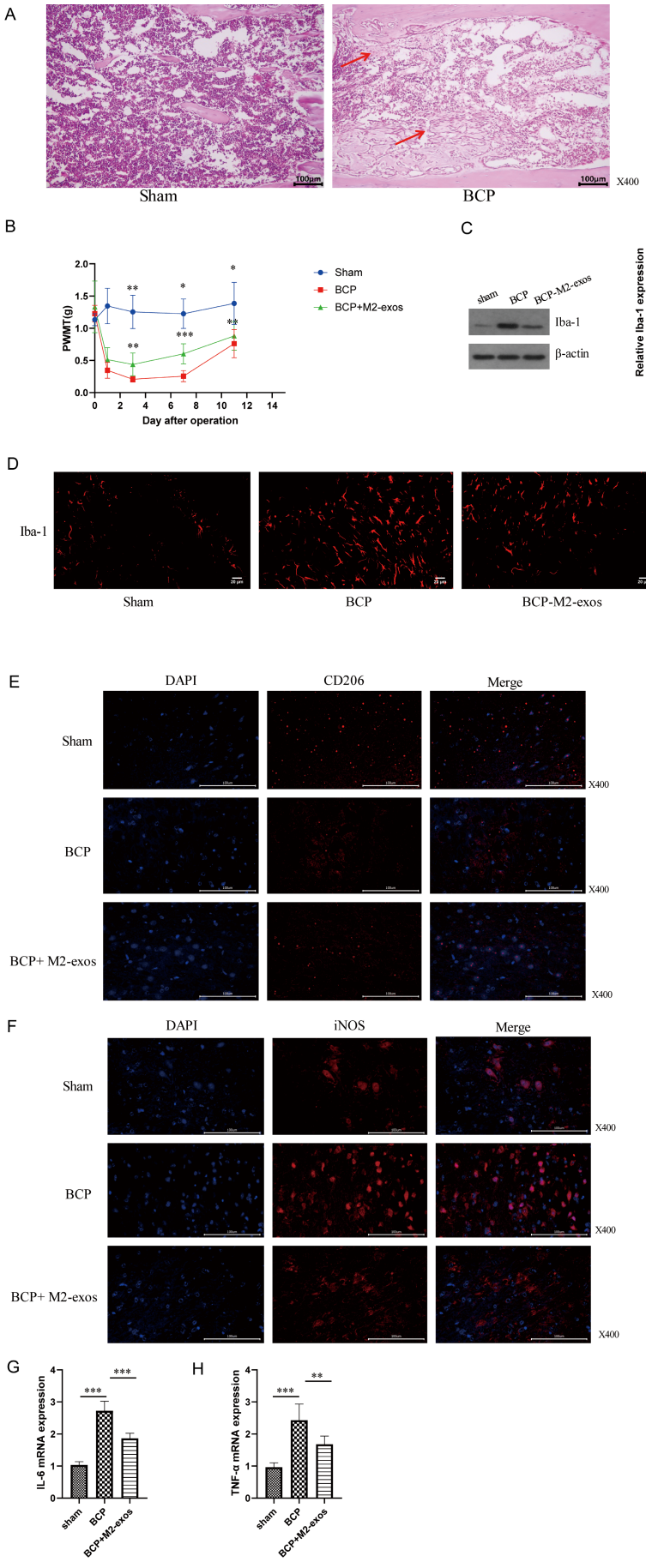
A
Sham
BCP
X400
B
PWMT(g)
Day after operation
Sham
BCP
BCP+M2-exos
C
sham
BCP
BCP-M2-exos
Iba-1
β-actin
Relative Iba-1 expression
D
Iba-1
Sham
BCP
BCP-M2-exos
X63
Relative fluorescence of Iba-1
E
DAPI
CD206
Merge
Sham
BCP
BCP+ M2-exos
X400
Relative fluorescence of CD206
F
DAPI
iNOS
Merge
Sham
BCP
BCP+ M2-exos
X400
Relative fluorescence of iNOS
G
IL-6 mRNA expression
H
TNF-α mRNA expression

Figure 3. M2-exos alleviated BCP progression in mice. (A) HE staining images showing the pathological changes in the sham mice and BCP mice, scale bars: 100 μm. (B) Mechanical allodynia of sham mice, BCP mice and BCP mice treated with M2-exos. (C) Expression of Iba-1 in the RVM in different experimental groups, as assessed by Western blotting. (D) Expression of Iba-1 in the RVM in different experimental groups, as detected by immunofluorescence, scale bars: 20 μm. The expression of the M2-like macrophage marker CD206 (E) and the M1-like macrophage marker iNOS (F) in the different experimental groups was analyzed by immunofluorescence, scale bars: 100 μm. mRNA expression of IL-6 (G) and TNF-α (H) in different experimental groups detected by qPCR. The data are presented as the mean ± SD; $^{*}P < 0.05$, $^{**}P < 0.01$, $^{***}P < 0.001$; n = 6.

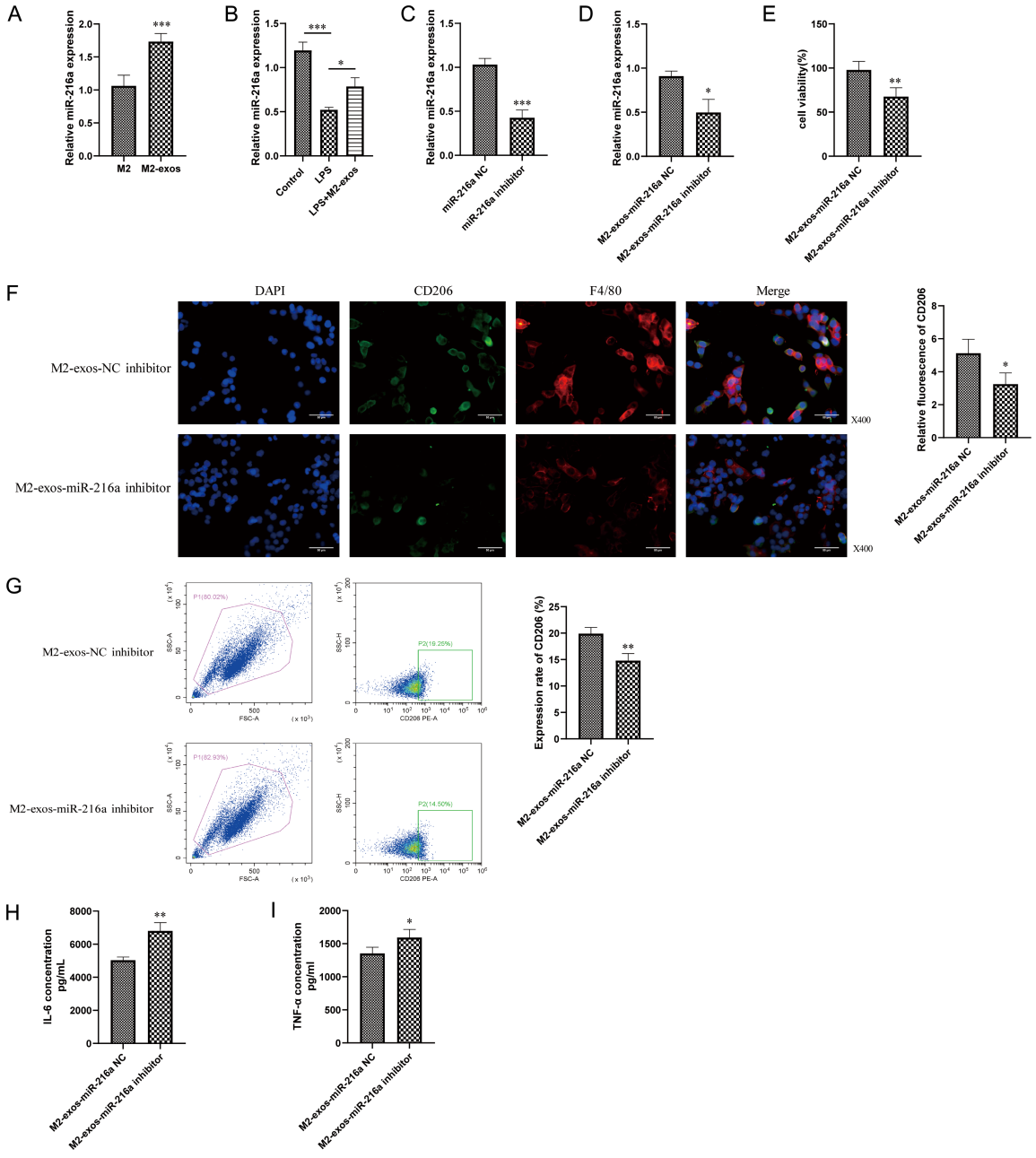

Figure 4. M2-exos transport miR-216a into BV2 cells and promote M2 polarization. (A) miR-216a expression in M2 macrophages and M2-exos was analyzed by qPCR. (B) miR-216a expression in BV2 cells, LPS-treated BV2 cells (BV2+LPS) and LPS-stimulated BV2 cells treated with M2-exos was detected by qPCR. (C) Expression of miR-216a in M2 macrophages transfected with the NC inhibitor or miR-216a inhibitor, as assessed by qPCR. (D) The expression of miR-216a in BV2 cells cocultured with M2-exos derived from NC or miR-216a-silenced M2 macrophages was detected by qPCR. (E) Viability of BV2 cells cocultured with M2-exos derived from NC or miR-216a-silenced M2 mac-

rophages, as assessed by a CCK-8 assay. (F) Immunofluorescence staining of CD206 in BV2 cells cocultured with M2-exos derived from NC or miR-216a-silenced M2 macrophages, scale bars: 50 μm. (G) Flow cytometry analysis of M2 microglia after coculture with M2-exos derived from NC or miR-216a-silenced M2 macrophages. Expression of IL-6 (H) and TNF-α (I) in BV2 cells cocultured with M2-exos derived from NC or miR-216a-silenced M2 macrophages. The data are presented as the mean ± SD; $^{*}P < 0.05$, $^{**}P < 0.01$, $^{***}P < 0.001$; n = 3.

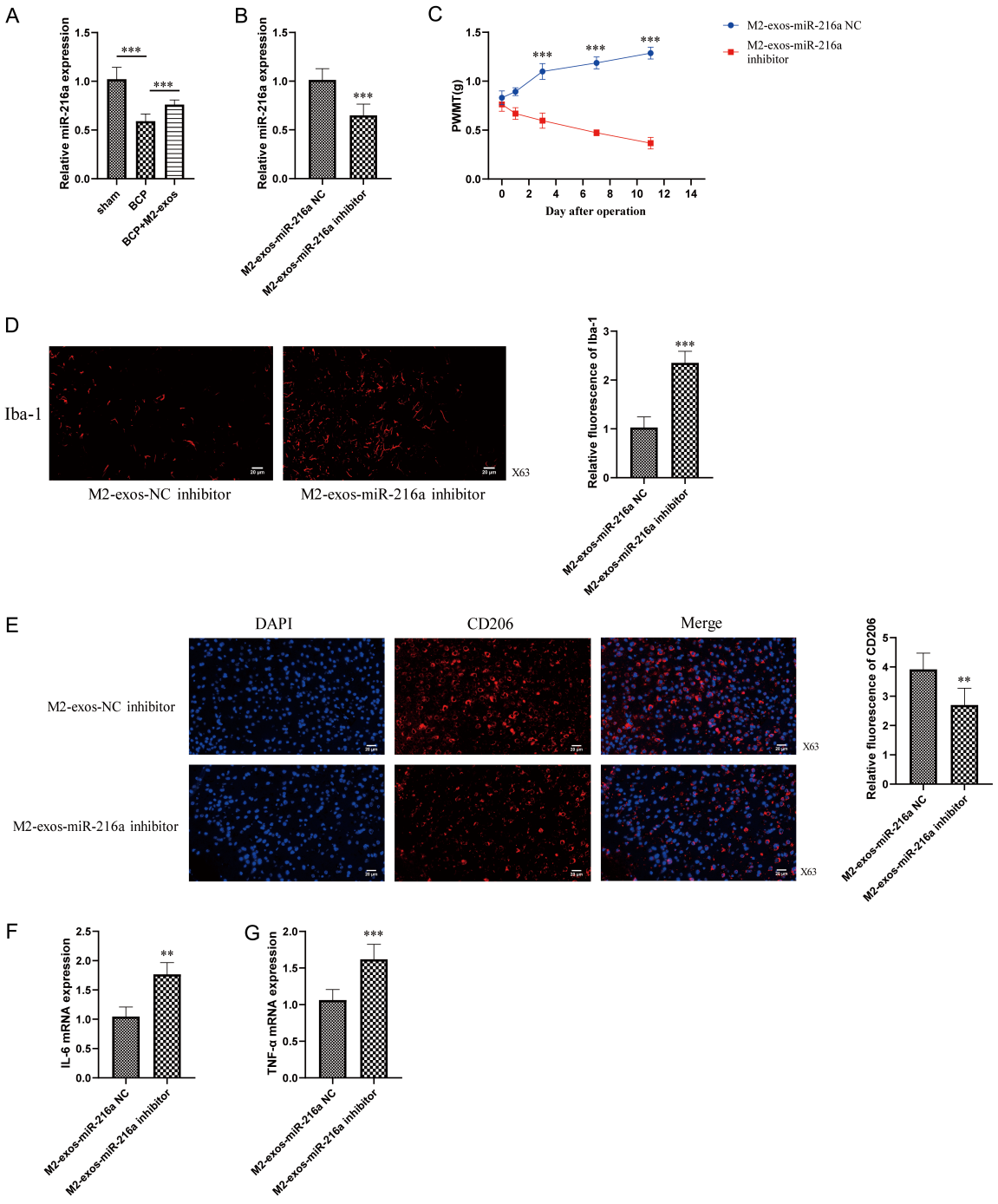

Figure 5. Exosomal miR-216a inhibited pain hypersensitivity and M2 microglial polarization in mice with BCP. (A) The expression of miR-216a in the RVM of sham mice, BCP mice and BCP mice treated with M2-exos was assessed by qPCR. (B) The expression of miR-216a in the RVM of BCP mice treated with exosomes derived from NC or miR-216a-silenced M2 macrophages was detected by qPCR. (C) Mechanical allodynia of BCP mice treated with exosomes derived from NC or miR-216a-silenced M2 macrophages. (D) Expression of Iba-1 in the RVM of mice with BCP treated

with exosomes derived from NC- or miR-216a-silenced M2 macrophages, as detected by immunofluorescence, scale bars: 20 μm. (E) CD206 expression in the RVM of mice with BCP treated with exosomes derived from NC- or miR-216a-silenced M2 macrophages was detected by immunofluorescence, scale bars: 20 μm. mRNA expression of IL-6 (F) and TNF-α (G) in different experimental groups detected by qPCR. The data are presented as the mean ± SD; $^{**}P < 0.01$, $^{***}P < 0.001$; n = 6.

kines was reversed upon miR-216a silencing (**Figure 5F** and **5G**).

Identification of HMGB1 as a target of miR-216a

miRNAs typically exert their biological functions by targeting downstream mRNAs. Bioinformatics analysis predicted HMGB1 as a potential target of miR-216a (**Figure 6A**), which was validated by dual-luciferase reporter assays (**Figure 6B**). In LPS-induced BV2 cells, HMGB1 expression was significantly upregulated (**Figure 6C**), whereas M2-exo treatment led to a decrease in HMGB1 levels (**Figure 6D**). Notably, when activated BV2 cells were treated with miR-216a-deficient M2-exos, HMGB1 expression was restored (**Figure 6E**), indicating that M2 macrophage-derived exosomal miR-216a exerts its effects via HMGB1.

Similarly, HMGB1 expression was elevated in mice with BCP but decreased following exosome microinjection. However, when exosomes with miR-216a knockdown were administered to BCP mice, HMGB1 expression levels were increased (**Figure 6F**).

Exosomal miR-216a blocked the TLR4/NF-κB signaling pathway

The TLR4/NF-κB signaling pathway plays a crucial role in HMGB1-mediated disease progression and has been implicated in BCP development. Therefore, we assessed the expression of TLR and NF-κB in both cells and the RVM of mice. In LPS-treated BV2 cells, the TLR4/NF-κB signaling pathway was activated (**Figure 7A**), whereas M2-exo treatment suppressed its activation (**Figure 7B**). However, M2-exos with miR-216a knockdown failed to inhibit the TLR4/NF-κB pathway in activated microglia (**Figure 7C**). In the RVM of mice with BCP, fluorescence signal of p65 in the nucleus and TLR4 were elevated but were reduced after M2-exo intervention (**Figure 7D** and **7E**). Upon inhibition of miR-216a in exosomes, fluorescence signal of p65 in the nucleus and TLR4 were restored (**Figure 7D** and **7E**).

Discussion

In this study, we demonstrated the therapeutic role of M2-exos in BCP and explored the possible underlying mechanisms. Our major findings are as follows. 1) M2-exos promoted M2 macrophage polarization and alleviated BCP progression. 2) M2-exos transported miR-216a and promoted M2 polarization in vivo and in vitro. 3) M2-exos induced M2 macrophage polarization and delayed BCP progression by regulating the HMGB1/TLR4/NF-κB pathway through the transport of miR-216a.

With the advancement of modern medical science, sophisticated medical technologies have significantly improved the long-term survival of an increasing number of cancer patients. Nevertheless, the concurrent pain symptoms experienced by these patients remain inadequately managed [1]. BCP is among the most common and distressing symptoms in cancer patients and has both neuropathic and inflammatory components [23]. Inadequate pain control often leads to psychological conditions such as depression and anxiety, a marked decline in quality of life, and an increased mortality risk [24, 25]. Therefore, the exploration of effective therapeutic strategies to alleviate BCP and increase patient survival remains a critical priority in clinical practice.

Neurons are considered the primary mediators of chronic pain. However, accumulating evidence highlights the significant role of neuroinflammation within the central nervous system, particularly the activation of glial cells such as microglia and astrocytes, in modulating chronic pain states [26]. The activation of glial cells and the subsequent release of inflammatory mediators may contribute to the initiation and maintenance of chronic pain [27]. Activated microglia are the major contributors to the development of inflammatory and neuropathic pain [28]. Microglial activation is heterogeneous and can be categorized into two types: the proinflammatory M1 phenotype and the anti-inflammatory M2 phenotype [29]. The

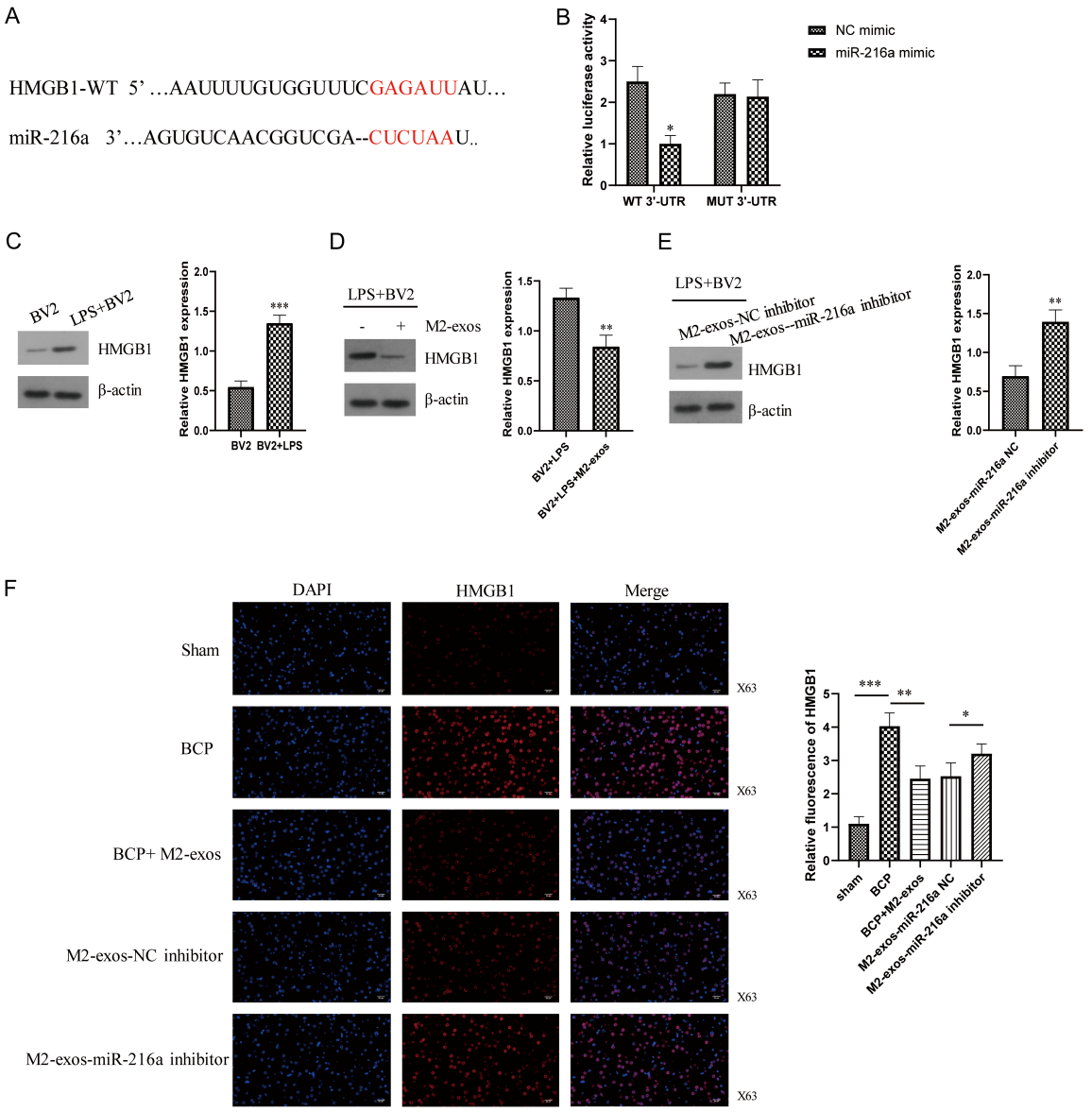

Figure 6. Identification of HMGB1 as a target of miR-216a. A. Prediction of binding sites between miR-216a and HMGB1. B. Dual-luciferase reporter assay of miR-216a and the HMGB1 mRNA 3' UTR binding sites. C. HMGB1 expression in BV2 cells and LPS-stimulated BV2 cells detected by Western blotting. D. Western blot analysis of HMGB1 expression in LPS-stimulated BV2 cells with/without M2-exo treatment. E. Expression of HMGB1 in LPS-stimulated BV2 cells cocultured with M2-exos derived from NC or miR-216a-silenced M2 macrophages, as assessed by Western blotting. F. HMGB1 expression in the RVM of sham mice, BCP mice, and BCP mice treated with exosomes derived from NC or miR-216a-silenced M2 macrophages was detected by immunofluorescence, scale bars: 20 μm. The data are presented as the mean ± SD; $^{*}P < 0.05$, $^{**}P < 0.01$, $^{***}P < 0.001$; n = 3; n = 6.

polarization of microglia plays a pivotal role in the pathogenesis and maintenance of chronic pain. Paeonol alleviates neuropathic pain by modulating microglial M1 and M2 polarization [30]. The inhibition of microglial M1 polarization attenuates neuropathic pain [31]. In contrast, the promotion of M2 microglial polarization can suppress neuropathic pain [32]. Thus, inducing microglial polarization toward the M2 phenotype represents a novel therapeutic strategy for chronic pain.

Compared with cell-based therapies, exosomes have advantages such as decreased infusion-related toxicity, low immunogenicity and high biocompatibility [33, 34]. Thus, they are widely

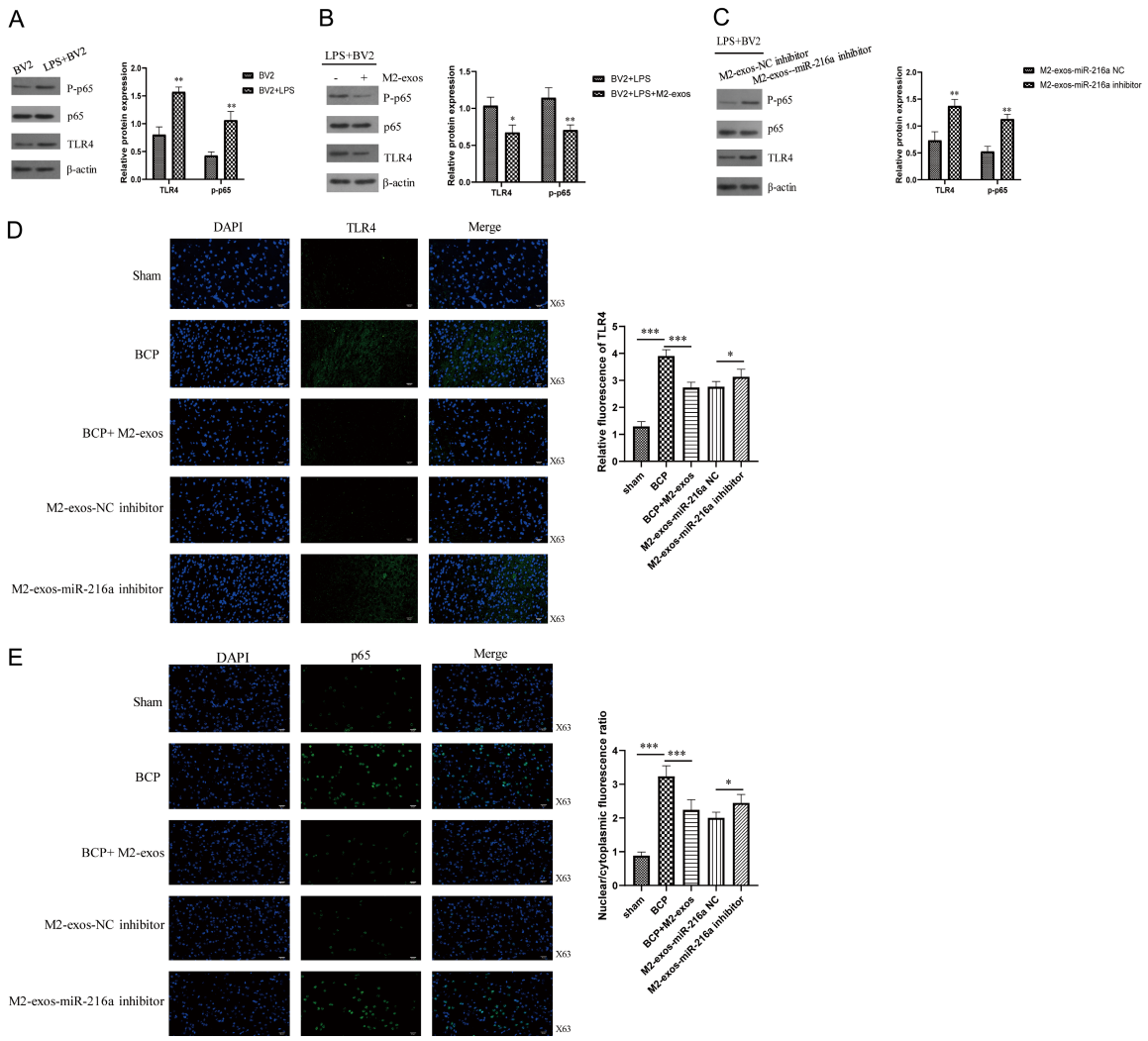

Figure 7. Exosomal miR-216a suppressed the TLR4/NF-κB signaling pathway. A. Expression of TLR4/NF-κB pathway-related proteins in BV2 cells and LPS-stimulated BV2 cells detected by Western blotting. B. Western blot analysis of the expression of TLR4/NF-κB pathway-related proteins in LPS-stimulated BV2 cells with/without M2-exo treatment. C. Western blot analysis of the expression of TLR4/NF-κB pathway-related proteins in LPS-stimulated BV2 cells co-cultured with M2-exos derived from NC or miR-216a-silenced M2 macrophages. D. Immunofluorescence analysis of TLR4 in the RVM of sham mice, BCP mice, and BCP mice treated with exosomes derived from NC or miR-216a-silenced M2 macrophages, as detected by immunofluorescence, scale bars: 20 μm. E. Immunofluorescence analysis of the nuclear translocation of NF-κB p65 in the RVM of sham mice, BCP mice, and BCP mice treated with exosomes derived from NC or miR-216a-silenced M2 macrophages, as detected by immunofluorescence, scale bars: 20 μm. The data are presented as the mean ± SD; $^{*}P < 0.05$, $^{**}P < 0.01$, $^{***}P < 0.001$; n = 3; n = 6.

used in fundamental and clinical studies. For example, exosomes derived from allogeneic bone marrow mesenchymal stem cells were used to treat patients with severe COVID-19 [35]. By encapsulating bioactive molecules such as lipids, nucleic acids and proteins, exosomes facilitate the transfer of biological information between cells, serving as key mediators in intercellular communication [36]. Exosomes have attracted extensive attention in the prediction and treatment of BCP [21, 37]. Previous studies have shown that exosomes can significantly affect macrophage polarization. Tumor-derived exosomes induce macrophage M2 polarization to promote colorectal cancer liver metastasis [38]. Exosomes from mesenchymal stem cells promote M2 macrophage polarization and inhibit periodontal bone loss [39]. M2 macrophages can mediate macrophage polarization through the release of exosomes [40].

Specifically, M2-exos promoted the polarization of macrophages toward the M2 rather than the M1 phenotype and attenuated inflammation [19]. In the present study, an in vitro neuroinflammation model was established using LPS-treated BV-2 cells, and a BCP mouse model was established by cancer cell injection. M2 macrophage-derived exosomes were isolated and characterized. M2-exos promoted microglial M2 polarization and alleviated the progression of BCP both in vivo and in vitro.

BCP is associated with microRNA dysregulation [41]. Accumulating evidence indicates that M2-exos exert therapeutic effects mainly through the delivery of miRNAs [42, 43]. On the basis of our previously published studies, we focused our investigation on miR-216a [22]. As a critical miRNA, miR-216a can suppress chronic pain through different pathways [44, 45]. Specifically, miR-216a functions upon its delivery via exosomes. Human urine-derived stem cell-derived exosomal miR-216a alleviates renal ischemia/reperfusion injury [46]. Bone marrow mesenchymal stem cell exosome-derived miR-216a attenuates neuronal injury and microglia-mediated inflammation [47]. In addition, exosomal miR-216a participates in the regulation of M1/M2 polarization [48]. Our study demonstrated that miR-216a was highly enriched in M2-exos and could be transferred into BV2 cells and BCP mice. miR-216a-silenced M2-exos impaired the ability of M2-exos to enhance microglial M2 polarization and alleviated the inhibitory effect of M2-exos on BCP progression. These results showed that M2-Exos delay BCP progression and regulate microglial polarization toward the M2 phenotype via delivery of miR-216a.

Exosomal miRNAs can regulate gene expression in recipient cells by binding to the 3' UTR of genes. On the basis of bioinformatics data and luciferase reporter assays, HMGB1 was determined to be the target gene of exosomal miR-216a. As a proinflammatory cytokine, HMGB1 plays a pivotal role in neuropathic and inflammatory pain [49, 50]. Thus, HMGB1 may serve as a therapeutic target for pain management. HMGB1 is a highly mobile nuclear protein that can interact with variety of cell surface receptors [51]. TLR4 is one of the receptors for HMGB1 which is expressed on microglia and mediates neuroinflammatory diseases [52]. Of note, HMGB1 and TLR-4 interactions may lead to NF-κB upregulation, which results in producing and releasing inflammatory cytokines [53]. HMGB1-mediated activation of the TLR4/NF-κB signaling pathway contributes to the progression of microglial activation and neuroinflammation [54, 55]. Moreover, the HMGB1/TLR4/NF-κB pathway widely influences microglial polarization [56]. These findings suggest that targeting the HMGB1/TLR4/NF-κB signaling axis may represent a promising therapeutic strategy for mitigating BCP. It is noteworthy that our previous research findings have demonstrated a correlation between M2-exos and both the TLR signaling pathway and the NF-κB signaling pathway [22]. The results of the present study revealed that the HMGB1/TLR4/NF-κB pathway was activated in LPS-stimulated BV2 cells and BCP mice and that treatment with M2-exos decreased the expression of HMGB1 and TLR4/NF-κB pathway-related molecules both in vitro and in vivo. The silencing of miR-216a largely reversed the exosomal miR-216a-mediated suppression of the HMGB1/TLR4/NF-κB signaling pathway.

Nevertheless, several limitations remain in the current study. For instance, miR-216a was selected as the primary focus based on prior sequencing data generated by the research team; however, other miRNAs identified in the same sequencing results may also contribute significantly to the observed biological effects, warranting further investigation. Furthermore, the present study was primarily conducted using in vitro cell cultures and animal models. Although the functional role of exosomes has been preliminarily elucidated, substantial challenges persist regarding their clinical translation. Specifically, the optimal dosage and timing of exosome-based interventions require additional systematic evaluation.

In summary, we conclude that M2-exos containing miR-216a promote the polarization of M1 microglia to the M2 phenotype by suppressing the HMGB1/TLR4/NF-κB-p65 signaling pathway, suggesting a potential therapeutic approach for the treatment of BCP.

Acknowledgements

This work was supported by the National Natural Science Foundation of China (82160229) and Yunnan Provincial Department of Science and Technology & Kunming Medical University

Joint Special Fund for Basic Research (2025-01AY070001-014).

Disclosure of conflict of interest

None.

Address correspondence to: Zhangxiang Huang and Qianye Li, Department of Pain, First Affiliated Hospital of Kunming Medical University, No. 295, Xichang Road, Wuhua District, Kunming 650000, Yunnan, China. Tel: +86-15697055158; E-mail: huangzhangxiang@kmmu.edu.cn (ZXH); Tel: +86-13700602193; E-mail: 13700602193@163.com (QYL)

References

[1] Patrick M. Bone cancer pain: causes, consequences, and therapeutic opportunities. Pain 2013; 154 Suppl 1: S54-S62.
[2] Yang L, Liu B, Zheng S, Xu L and Yao M. Understanding the initiation, delivery and processing of bone cancer pain from the peripheral to the central nervous system. Neuropharmacology 2023; 237: 109641.
[3] Wang K, Gu Y, Liao Y, Bang S, Donnelly CR, Chen O, Tao X, Mirando AJ, Hilton MJ and Ji RR. PD-1 blockade inhibits osteoclast formation and murine bone cancer pain. J Clin Invest 2020; 130: 3603-3620.
[4] Denis RC and Patrick WM. Bone cancer pain. Cancer 2003; 97.
[5] Lucchesi M, Lanzetta G, Antonuzzo A, Rozzi A, Sardi I, Favre C, Ripamonti CI, Santini D and Armento G. Developing drugs in cancer-related bone pain. Crit Rev Oncol Hematol 2017; 119: 66-74.
[6] Nguyen QN, Chun SG, Chow E, Komaki R, Liao Z, Zacharia R, Szeto BK, Welsh JW, Hahn SM, Fuller CD, Moon BS, Bird JE, Satcher R, Lin PP, Jeter M, O'Reilly MS and Lewis VO. Single-fraction stereotactic vs conventional multifraction radiotherapy for pain relief in patients with predominantly nonspine bone metastases: a randomized phase 2 trial. JAMA Oncol 2019; 5: 872-878.
[7] Chu X, Zhuang H, Liu Y, Li J, Wang Y, Jiang Y, Zhang H, Zhao P, Chen Y, Jiang X, Wu Y and Bu W. Blocking cancer-nerve crosstalk for treatment of metastatic bone cancer pain. Adv Mater 2022; 34: e2108653.
[8] Huang ZX, Lu ZJ, Ma WQ, Wu FX, Zhang YQ, Yu WF and Zhao ZQ. Involvement of RVM-expressed P2X7 receptor in bone cancer pain: mechanism of descending facilitation. Pain 2014; 155: 783-791.
[9] Liu X, Bu H, Liu C, Gao F, Yang H, Tian X, Xu A, Chen Z, Cao F and Tian Y. Inhibition of glial activation in rostral ventromedial medulla attenuates mechanical allodynia in a rat model of cancer-induced bone pain. J Huazhong Univ Sci Technolog Med Sci 2012; 32: 291-298.
[10] Tsuda M. Microglia in the CNS and neuropathic pain. Adv Exp Med Biol 2018; 1099: 77-91.
[11] Atta AA, Ibrahim WW, Mohamed AF and Abdelkader NF. Microglia polarization in nociplastic pain: mechanisms and perspectives. Inflammopharmacology 2023; 31: 1053-1067.
[12] Zhang LQ, Gao SJ, Sun J, Li DY, Wu JY, Song FH, Liu DQ, Zhou YQ and Mei W. DKK3 ameliorates neuropathic pain via inhibiting ASK-1/JNK/p-38-mediated microglia polarization and neuroinflammation. J Neuroinflammation 2022; 19: 129.
[13] Liu L, Li DY, Zhang LQ, Gao SJ, Song FH, Wu JY, Zhou YQ, Liu DQ and Mei W. Administration of 2-deoxy-D-glucose alleviates cancer-induced bone pain by suppressing microglial polarization to the M1 phenotype and neuroinflammation. Mol Pain 2025; 21: 17448069251348778.
[14] Zhang J, Li S, Li L, Li M, Guo C, Yao J and Mi S. Exosome and exosomal microRNA: trafficking, sorting, and function. Genomics Proteomics Bioinformatics 2015; 13: 17-24.
[15] Krylova SV and Feng D. The machinery of exosomes: biogenesis, release, and uptake. Int J Mol Sci 2023; 24: 1337.
[16] Zhang L and Yu D. Exosomes in cancer development, metastasis, and immunity. Biochim Biophys Acta Rev Cancer 2019; 1871: 455-468.
[17] Huang LH, Rau CS, Wu SC, Wu YC, Wu CJ, Tsai CW, Lin CW, Lu TH and Hsieh CH. Identification and characterization of hADSC-derived exosome proteins from different isolation methods. J Cell Mol Med 2021; 25: 7436-7450.
[18] Xian X, Cai LL, Li Y, Wang RC, Xu YH, Chen YJ, Xie YH, Zhu XL and Li YF. Neuron secrete exosomes containing miR-9-5p to promote polarization of M1 microglia in depression. J Nanobiotechnology 2022; 20: 122.
[19] Zhang Y, Zhu L, Li X, Ge C, Pei W, Zhang M, Zhong M, Zhu X and Lv K. M2 macrophage exosome-derived lncRNA AK083884 protects mice from CVB3-induced viral myocarditis through regulating PKM2/HIF-1α axis mediated metabolic reprogramming of macrophages. Redox Biol 2024; 69: 103016.
[20] Gurung S, Perocheau D, Touramanidou L and Baruteau J. The exosome journey: from biogenesis to uptake and intracellular signalling. Cell Commun Signal 2021; 19: 47.
[21] Khasabova IA, Khasabov SG, Johns M, Juliette J, Zheng A, Morgan H, Flippen A, Allen K, Go-

lovko MY, Golovko SA, Zhang W, Marti J, Cain D, Seybold VS and Simone DA. Exosome-associated lysophosphatidic acid signaling contributes to cancer pain. Pain 2023; 164: 2684-2695.
[22] Cai X, Xi X, Li X, Zhang X, Zhang X, Huang Z and Yan Z. Antinociceptive effects of macrophage-derived extracellular vesicles by carrying microRNA-216a. Am J Transl Res 2021; 13: 1971-1989.
[23] Bao Y, Gao Y, Hou W, Yang L, Kong X, Zheng H, Li C and Hua B. Engagement of signaling pathways of protease-activated receptor 2 and μ-opioid receptor in bone cancer pain and morphine tolerance. Int J Cancer 2015; 137: 1475-83.
[24] Liu S, Zhu R, Zhang Y, Jiang Z, Chen Y, Song Q and Wang F. Targeting PI3K-mTOR signaling in the anterior cingulate cortex improves emotional behavior, and locomotor activity in rats with bone cancer pain. Ann Med Surg (Lond) 2025; 87: 1985-1994.
[25] Falk S and Dickenson AH. Pain and nociception: mechanisms of cancer-induced bone pain. J Clin Oncol 2014; 32: 1647-54.
[26] Ji RR, Xu ZZ and Gao YJ. Emerging targets in neuroinflammation-driven chronic pain. Nat Rev Drug Discov 2014; 13: 533-48.
[27] Zhou YQ, Liu Z, Liu HQ, Liu DQ, Chen SP, Ye DW and Tian YK. Targeting glia for bone cancer pain. Expert Opin Ther Targets 2016; 20: 1365-1374.
[28] Yang Y, Li H, Li TT, Luo H, Gu XY, Lü N, Ji RR and Zhang YQ. Delayed activation of spinal microglia contributes to the maintenance of bone cancer pain in female Wistar rats via P2X7 receptor and IL-18. J Neurosci 2015; 35: 7950-63.
[29] Orihuela R, McPherson CA and Harry GJ. Microglial M1/M2 polarization and metabolic states. Br J Pharmacol 2016; 173: 649-65.
[30] Li X, Shi H, Zhang D, Jing B, Chen Z, Zheng Y, Chang S, Gao L and Zhao G. Paeonol alleviates neuropathic pain by modulating microglial M1 and M2 polarization via the RhoA/p38MAPK signaling pathway. CNS Neurosci Ther 2023; 29: 2666-2679.
[31] Wu W, Zhang X, Wang S, Li T, Hao Q, Li S, Yao W and Sun R. Pharmacological inhibition of the cGAS-STING signaling pathway suppresses microglial M1-polarization in the spinal cord and attenuates neuropathic pain. Neuropharmacology 2022; 217: 109206.
[32] Wu Q, Zheng Y, Yu J, Ying X, Gu X, Tan Q, Tu W, Lou X, Yang G, Li M and Jiang S. Electroacupuncture alleviates neuropathic pain caused by SNL by promoting M2 microglia polarization through PD-L1. Int Immunopharmacol 2023; 123: 110764.
[33] Lotfy A, AboQuella NM and Wang H. Mesenchymal stromal/stem cell (MSC)-derived exosomes in clinical trials. Stem Cell Res Ther 2023; 14: 66.
[34] Wu W, Zhang B, Wang W, Bu Q, Li Y, Zhang P and Zeng L. Plant-derived exosome-like nanovesicles in chronic wound healing. Int J Nanomedicine 2024; 19: 11293-11303.
[35] Sengupta V, Sengupta S, Lazo A, Woods P, Nolan A and Bremer N. Exosomes derived from bone marrow mesenchymal stem cells as treatment for severe COVID-19. Stem Cells Dev 2020; 29: 747-754.
[36] Dad HA, Gu TW, Zhu AQ, Huang LQ and Peng LH. Plant exosome-like nanovesicles: emerging therapeutics and drug delivery nanoplatforms. Mol Ther 2021; 29: 13-31.
[37] Li X, Chen Y, Wang J, Jiang C and Huang Y. Lung cancer cell-derived exosomal let-7d-5p downregulates OPRM1 to promote cancer-induced bone pain. Front Cell Dev Biol 2021; 9: 666857.
[38] Zhao S, Mi Y, Guan B, Zheng B, Wei P, Gu Y, Zhang Z, Cai S, Xu Y, Li X, He X, Zhong X, Li G, Chen Z and Li D. Tumor-derived exosomal miR-934 induces macrophage M2 polarization to promote liver metastasis of colorectal cancer. J Hematol Oncol 2020; 13: 156.
[39] Nakao Y, Fukuda T, Zhang Q, Sanui T, Shinjo T, Kou X, Chen C, Liu D, Watanabe Y, Hayashi C, Yamato H, Yotsumoto K, Tanaka U, Taketomi T, Uchiumi T, Le AD, Shi S and Nishimura F. Corrigendum to "Exosomes from TNF-α-treated human gingiva-derived MSCs enhance M2 macrophage polarization and inhibit periodontal bone loss" [Acta Biomaterialia 2021, 122, 306-324]. Acta Biomater 2025; 191: 428-429.
[40] Qian Y, Chu G, Zhang L, Wu Z, Wang Q, Guo JJ and Zhou F. M2 macrophage-derived exosomal miR-26b-5p regulates macrophage polarization and chondrocyte hypertrophy by targeting TLR3 and COL10A1 to alleviate osteoarthritis. J Nanobiotechnology 2024; 22: 72.
[41] Bali KK, Selvaraj D, Satagopam VP, Lu J, Schneider R and Kuner R. Genome-wide identification and functional analyses of microRNA signatures associated with cancer pain. EMBO Mol Med 2013; 5: 1740-58.
[42] Ying W, Gao H, Dos Reis FCG, Bandyopadhyay G, Ofrecio JM, Luo Z, Ji Y, Jin Z, Ly C and Olefsky JM. MiR-690, an exosomal-derived miRNA from M2-polarized macrophages, improves insulin sensitivity in obese mice. Cell Metab 2021; 33: 781-790, e5.
[43] Yang Y, Guo Z, Chen W, Wang X, Cao M, Han X, Zhang K, Teng B, Cao J, Wu W, Cao P, Huang C and Qiu Z. M2 macrophage-derived exosomes promote angiogenesis and growth of pancre-

atic ductal adenocarcinoma by targeting E2F2. Mol Ther 2021; 29: 1226-1238.
[44] Wang W and Li R. MiR-216a-5p alleviates chronic constriction injury-induced neuropathic pain in rats by targeting KDM3A and inactivating Wnt/β-catenin signaling pathway. Neurosci Res 2021; 170: 255-264.
[45] Xin Y, Song X and Ge Q. Circular RNA SMEK1 promotes neuropathic pain in rats through targeting microRNA-216a-5p to mediate Thioredoxin Interacting Protein (TXNIP) expression. Bioengineered 2021; 12: 5540-5551.
[46] Zhang Y, Wang J, Yang B, Qiao R, Li A, Guo H, Ding J, Li H, Ye H, Wu D, Cui L and Yang S. Transfer of microRNA-216a-5p from exosomes secreted by human urine-derived stem cells reduces renal ischemia/reperfusion injury. Front Cell Dev Biol 2020; 8: 610587.
[47] Xue H, Ran B, Li J, Wang G, Chen B and Mao H. Bone marrow mesenchymal stem cell exosomes-derived microRNA-216a-5p on locomotor performance, neuronal injury, and microglia inflammation in spinal cord injury. Front Cell Dev Biol 2023; 11: 1227440.
[48] Liu W, Rong Y, Wang J, Zhou Z, Ge X, Ji C, Jiang D, Gong F, Li L, Chen J, Zhao S, Kong F, Gu C, Fan J and Cai W. Exosome-shuttled miR-216a-5p from hypoxic preconditioned mesenchymal stem cells repair traumatic spinal cord injury by shifting microglial M1/M2 polarization. J Neuroinflammation 2020; 17: 47.
[49] Li M, Jiang H, Gu K, Sun X, Gu J, Li C and Wang G. Lidocaine alleviates neuropathic pain and neuroinflammation by inhibiting HMGB1 expression to mediate MIP-1α/CCR1 pathway. J Neuroimmune Pharmacol 2021; 16: 318-333.
[50] Zhang X, Zhao W, Liu X, Huang Z, Shan R and Huang C. Celastrol ameliorates inflammatory pain and modulates HMGB1/NF-κB signaling pathway in dorsal root ganglion. Neurosci Lett 2019; 692: 83-89.
[51] Sims GP, Rowe DC, Rietdijk ST, Herbst R and Coyle AJ. HMGB1 and RAGE in inflammation and cancer. Annu Rev Immunol 2010; 28: 367-88.
[52] Le K, Chibaatar Daliv E, Wu S, Qian F, Ali AI, Yu D and Guo Y. SIRT1-regulated HMGB1 release is partially involved in TLR4 signal transduction: a possible anti-neuroinflammatory mechanism of resveratrol in neonatal hypoxic-ischemic brain injury. Int Immunopharmacol 2019; 75: 105779.
[53] Yang QW, Lu FL, Zhou Y, Wang L, Zhong Q, Lin S, Xiang J, Li JC, Fang CQ and Wang JZ. HMBG1 mediates ischemia-reperfusion injury by TRIF-adaptor independent Toll-like receptor 4 signaling. J Cereb Blood Flow Metab 2011; 31: 593-605.
[54] Xu X, Piao HN, Aosai F, Zeng XY, Cheng JH, Cui YX, Li J, Ma J, Piao HR, Jin X and Piao LX. Arctigenin protects against depression by inhibiting microglial activation and neuroinflammation via HMGB1/TLR4/NF-κB and TNF-α/TNFR1/NF-κB pathways. Br J Pharmacol 2020; 177: 5224-5245.
[55] Zhang Z, Jiang J, He Y, Cai J, Xie J, Wu M, Xing M, Zhang Z, Chang H, Yu P, Chen S, Yang Y, Shi Z, Liu Q, Sun H, He B, Zeng J, Huang J, Chen J, Li H, Li Y, Lin WJ and Tang Y. Pregabalin mitigates microglial activation and neuronal injury by inhibiting HMGB1 signaling pathway in radiation-induced brain injury. J Neuroinflammation 2022; 19: 231.
[56] Wu J, Hao Z, Wang Y, Yan D, Meng J and Ma H. Melatonin alleviates BDE-209-induced cognitive impairment and hippocampal neuroinflammation by modulating microglia polarization via SIRT1-mediated HMGB1/TLR4/NF-κB pathway. Food Chem Toxicol 2023; 172: 113561.